Vibration Analysis and Stability Prediction for CNC End-Milling

by

Neel D. Shah

Department of Mechanical Engineering and Materials Science
Duke University

Date: _____

Approved:

_____
Brian Mann, Supervisor

_____
Samuel Stanton

_____
Chuan-Hua Chen

Thesis submitted in partial fulfillment of the requirements for the degree of Master of Science in the Department of Mechanical Engineering and Materials Science
in the Graduate School of Duke University
2018

Abstract

Vibration Analysis and Stability Prediction for CNC End-Milling

by

Neel D. Shah

Department of Mechanical Engineering and Materials Science
Duke University

Date: _____

Approved:

_____
Brian Mann, Supervisor

_____
Samuel Stanton

_____
Chuan-Hua Chen

An abstract of a thesis submitted in partial fulfillment of the requirements for the degree of Master of Science in the Department of Mechanical Engineering and Materials Science
in the Graduate School of Duke University
2018

Abstract

This Master's Thesis investigates the process of stability prediction for milling process. Stability prediction for a given tool-workpiece combination can maximize material removal rate while maintaining vibrational stability. Milling is modelled as a time-delayed system with single degree of freedom. Temporal Finite Element Analysis & Spectral Element Analysis algorithms have been prepared to solve those. TFEA algorithm is then customized for milling process to prepare stability charts for a given system.

The algorithm is verified by experimental means. A compliant system is designed and manufactured for cutting tests. Impact modal tests are performed to extract modal parameters, which are used to produce stability charts. Milling test passes are done on the workpiece for various combinations of spindle speeds and depths of cut. Real-time workpiece displacement and spindle speed data is used to identify stability of the cuts. These are then analyzed and compared with stability predictions.

The findings of this work indicate considerable agreement of theory with experiment. TFEA algorithm was able to predict stability accurately for low spindle speeds. They also suggest the need to consider dynamics of the cutting tool and to model a second degree of freedom for more accurate predictions.

Contents

List of Tables

List of Figures

List of Abbreviations and Symbols

Symbols

m	Modal mass.
c	Damping coefficient
ζ	Damping ratio
K	Stiffness
τ	Time delay
ω_n	Natural frequency
ω_d	Damped natural frequency
Ω	Angular velocity of spindle
x	Linear displacement
$\dot{x}$	Velocity
$\ddot{x}$	Acceleration
F_t	Tangential force
F_n	Normal force
w	Chip thickness
x	Linear displacement
$\dot{x}$	Velocity
σ_j	Local element time

Abbreviations

MRR	Material Removal Rate
DDE	Delay-Differential Equation
TFEA	Temporal Finite Element Analysis
SEA	Spectral Element Analysis
SDOF	Single Degree of Freedom
CM	Characteristic Multiplier
LGL	Legendre Gauss Lobatto
CNC	Computer Numerical Control
DAQ	Data Acquisition
FFT	Fast Fourier Transform
FRF	Frequency Response Function

Acknowledgements

During my time at Duke University, I have had the pleasure to work with Dr. Brian Mann. Two graduate courses and full-time academic research with him have been a steep learning curve. I would like to thank him for all the resources, research exposure, guidance and constant support. I would also like to thank Jared Little, PhD student in the Dynamical Systems Lab. He has been of great help with the literature review, experiment design and troubleshooting.

I would also like to thank the staff at Duke University's CoLab and Student Machine shop for always being supportive and proactive to help. Lastly, I am thankful to my committee members: Dr. Samuel Stanton, Dr. Chuan-Hua Chen and Dr. Brian Mann for their helpful suggestions and support.

1

Introduction

1.1 Motivation

Milling is one of the major industrial processes used for production of finished metal parts, following bulk deformation [1]. Its performance can be characterized by a set of final product characteristics that include dimensional accuracy, machining time and surface quality. With globalization and increased industrial competition, cost control has become very crucial, while maintaining product quality. In milling, cost is majorly dependent on the process time, which includes set-up time, transfer time, and most importantly, machining time. Machining time is significantly dependent on machining parameters such as spindle speed and depth of cut, which in turn determine the Material Removal Rate (MRR).

The machining parameters are limited by undesirable self-excited vibrations at the tool-workpiece interface, called chatter. It is known to cause significant dynamic loads on the workpiece, tool, and machine structure. This leads to lower surface quality and damage to cutting tool [2]. Even some stable vibrations cause surface location errors, and hence dimensional inaccuracy. Therefore, it is important to set a right combination of machining parameters to avoid either.

Conventionally, parameter selection is done by trial and error, which is both cost and time intensive. Instead, the availability of predictive dynamic models for a given combination of tool-workpiece combination can help identify regions of stable and unstable cutting for a large combination of machining parameters. This allows manufacturers to produce parts with same, or better quality and increased MRR, and subsequently reduced costs. Since milling is one of the most widely used manufacturing processes, development of its predictive model and experimental verification has become my research focus.

1.2 Thesis Outline

This thesis discusses theoretical and experimental aspects of the prescribed problem statement. The goal is development and verification of algorithm to produce stability charts for a given tool-workpiece combination. First step towards this is development of mechanical model of the physical system. The resulting mathematical equations are in the form of Delay-Differential Equations (DDEs) [3][4]. Considerable research has been done on analytical approach for these DDEs, for both continuous and intermittent forcing functions. This thesis goes through development of Temporal Finite Element Analysis (TFEA) and Spectral Element Analysis (SEA) for solving these equations and producing stability charts. Further, their convergence and performance as algorithm are compared. In this thesis, a TFEA algorithm has been developed for the case of end-milling with a tool helix angle. The next chapter covers all the above mentioned topics.

Third chapter focuses on experimental validation of the theoretical development that was done in Ch. 2. For the assumed Single Degree of Freedom (SDOF) model, a set-up was designed which was compliant in only one direction. Impact hammer modal tests were performed on it and modal parameters extracted. They were then used to prepare stability charts with ranges of spindle speeds and depths of cut.

Cutting tests were then performed on the workpiece for various combinations of machining parameters. Vibration data from the cutting tests was analyzed and compared with the predicted dynamic characteristics.

2

Analytical Approach to Stability Prediction

2.1 Mathematical model of milling

For the purpose of vibration analysis, the tool-workpiece combination is assumed to be a SDOF system. Considering other forces to be negligible, only the cutting tool is responsible for forcing the system. Figure 2.1 shows a schematic of the modelled system, along with the cutting forces. The workpiece is flexible along a direction orthogonal to feed direction. F_t, F_n, C_y and K_y represent tangential force, normal force, damping and stiffness, respectively. RI refers to the radial immersion.

Similar to a forced SDOF oscillator, the fundamental equation of motion of the system can be given by the following equation

$$m\ddot{x} + c\dot{x} + kx = F(t, \tau) \tag{2.1}$$

or

$$\ddot{x} + 2\zeta\omega_n\dot{x} + {\omega_n}^2 x = \frac{1}{m}F(t, \tau) \tag{2.2}$$

where m is the modal mass, ω_n is the natural frequency, ζ is the damping ratio, and $\tau = 60/\Omega$ is the time period of one rotation for the tool. Ω is the spindle speed in

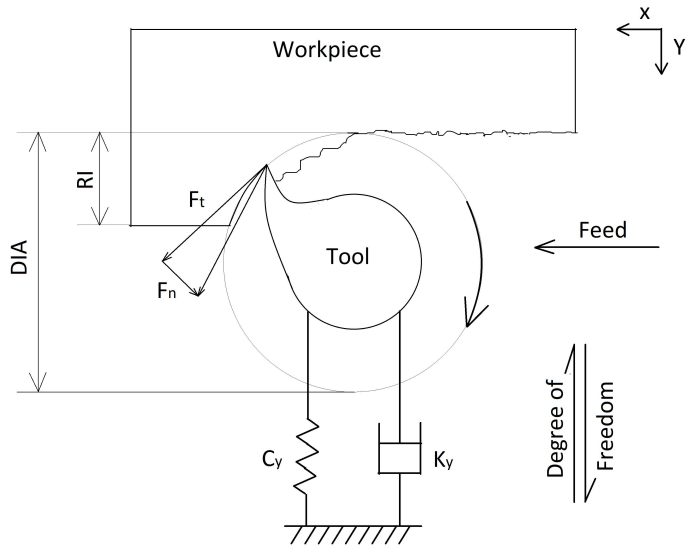

FIGURE 2.1: Schematic diagram of the tool-workpiece interface for a SDOF down-milling process with compliance in the y-direction.

RPM. $F(t,\tau)$ is the intermittent cutting force that depends on both the time and the time delay between consecutive passages of the cutting teeth.

Cutting force consists of two components, normal and tangential. Since the cutting operation is not continuous, tooth is not always in contact with the workpiece. Hence, the force switches between zero and non-zero values, depending on the cutting edge's entry and exit angles. The forcing function can be rewritten as

$$F(t,\tau) = -\delta(t)[F_t(t,\tau)cos\theta(t) + F_n(t,\tau)sin\theta(t)] \tag{2.3}$$

where $\delta(t)$ is a unit step function. It is unity when a cutting tooth is in contact with the workpiece and zero when it is not. F_t and F_n are tangential and normal components of the force, respectively. $\theta(t)$ is the angular position of the cutting edge. The force components depend on cutting coefficients K_t and K_n, depth of cut w and

radial chip width z [4]. They can be written as

$$\begin{aligned} F_t(t,\tau) &= K_t w z(t,\tau) \\ F_n(t,\tau) &= K_n w z(t,\tau) \end{aligned} \tag{2.4}$$

From previous works [5], a circular cutting-edge path can be assumed. The radial chip width depends on travel per tooth, tool angle and regeneration. According to [6], it can be given by

$$z(t,\tau) = h sin\theta(t) + [x(t) - x(t-\tau)] sin\theta(t) \tag{2.5}$$

The forcing term can now be written as

$$\begin{aligned} F = -\delta_p(t)[K_t cos\theta_p(t) + K_n sin\theta_p(t)] sin\theta_p(t) w[x(t) - x(t-\tau)] \\ -w.\delta_p(t)[K_t cos\theta_p(t) + K_n sin\theta_p(t)] h sin\theta_p(t) \end{aligned} \tag{2.6}$$

which can be simplified to the form

$$F = -C_1(t) w[x(t) - x(t-\tau)] - C_2(t) w \tag{2.7}$$

C_1 and C_2 can be represented as

$$C_1(t) = \delta(t)[K_t cos\theta(t) + K_n sin\theta(t)] sin\theta(t) \tag{2.8}$$

$$C_2(t) = \delta(t)[K_t cos\theta(t) + K_n sin\theta(t)] h sin\theta(t) \tag{2.9}$$

The term $C_1(t)$ is periodic in nature and it dictates stability depending on the perturbations about system's motion. $C_2(t)$ is also periodic, but governs the forcing in the absence of time-delayed excitation.

Stability Analysis

It has been known that milling operation can be described as a model that includes past effects. These models can be represented by delay differential equations (DDEs)

in which the rate of change of present state depends on both the past and the present states. The general form of a linear autonomous DDE is

$$\dot{x}(t) = \mathbf{A}x(t) + \mathbf{B}x(t-\tau), \tag{2.10}$$

where $\mathbf{A}$ & $\mathbf{B}$ are square matrices and $\tau > 0$. Matrix dimensions are dictated by order of the equation. An exponential solution leads to a characteristic equation that can be written as

$$\left|\lambda\mathbf{I} - \mathbf{A} - \mathbf{B}e^{-\lambda\tau}\right| = 0, \tag{2.11}$$

For asymptotic stability, all the characteristic roots need to have a negative real parts [7]. Hence, the above form can be reduced to

$$\mathbf{y_n} = \mathbf{M}\mathbf{y}_{n-1}, \tag{2.12}$$

where y_n is the state variable at current period and y_{n-1} is the state variable at the previous delay period. For asymptotic stability, all the characteristic multipliers of $\mathbf{M}$ need to have a magnitude of less than one. Considering a similar system, Equation 2.10 can be rewritten as

$$\dot{\mathbf{y}}(t) = \mathbf{A}(t)\mathbf{y}(t) + \mathbf{B}(t)\mathbf{y}(t-\tau), \tag{2.13}$$

where $\mathbf{A}$ and $\mathbf{B}$ have a period of T, i.e. $\mathbf{A}(t) = \mathbf{A}(t+T)$ and $\mathbf{B}(t) = \mathbf{B}(t+T)$. Similarly, the solution can also be written in a periodic form where $\mathbf{y} = \mathbf{p}(t)e^t$, $\mathbf{p}(t) = \mathbf{p}(t+T)$. An important note is that the monodromy operator [8] $\mathbf{M}$ has infinite dimensions, unlike the classic time period cases. Since a closed-form solution is not possible because of this infinite dimensionality, a finite-dimensional monodromy operator can be defined, which satisfactorily approximates the exact infinite-dimensional monodromy operator.

The math model can be solved by various methods, two of those being Temporal Finite Element Analysis (TFEA) and Spectral Element Analysis (SEA). Both of these will be discussed in upcoming sections.

2.2 Temporal Finite Element Analysis

This section applies TFEA for stability prediction of a milling operation. The method was developed first by Bayly et. al [9] for turning process. Unlike turning, which is a continuous cutting process, milling is an intermittent cutting process. For milling, the time of one spindle revolution can be divided in two time periods - when cutting tooth is in contact with the workpiece, and when it is not. The former leads to forced vibration, whereas the latter leads to free vibrations. Hence, the DDEs are solved separately for both and then approximately solved to produce the final stability charts.

2.2.1 Forced Vibrations

When the cutting tooth is in contact with the workpiece, it is forced vibration which is governed by a time DDE, as discussed in previous section. According to [4], an approximate solution for tool displacement is assumed which is of the form

$$x(t) = \sum_{i=1}^{4} a_{ji}^{n} \phi_i(\sigma_j(t)), \tag{2.14}$$

The above form of displacement refers to that of j^{th} element of n^{th} period. The term $\sigma_j(t)$ is the local time for the given element which can be represented as

$$\sigma_j(t) = t - n\tau \sum_{k=1}^{j-1} t_k, \tag{2.15}$$

Since the assumed solution is an approximation, substituting it in the equation of motion will produce a non-zero error $\varepsilon(t)$ given by

$$\begin{aligned} &m\left(\sum_{i=1}^{4} a_{ji}^{n} \ddot{\phi}_i(t)\right) + c\left(\sum_{i=1}^{4} a_{ji}^{n} \dot{\phi}_i(t)\right) + k\left(\sum_{i=1}^{4} a_{ji}^{n} \phi_i(t)\right) \\ -wC_1(t)&\left[\left(\sum_{i=1}^{4} a_{ji}^{n} \phi_i(t)\right) - \left(\sum_{i=1}^{4} a_{ji}^{n-1} \phi_i(t)\right)\right] - wC_2(t) = \varepsilon(t), \end{aligned} \tag{2.16}$$

Two test functions are chosen such that the assumed solution can be weighted by multiplication with those functions, and the error is reduced to zero. They are

$$\begin{aligned} \psi_1(\sigma_j) &= 1, \\ \psi_2(\sigma_j) &= \frac{\sigma_j}{t_j} - \frac{1}{2}. \end{aligned} \tag{2.17}$$

The four trial functions, or Hermite functions, $\phi_i(\sigma_j(t))$ on jth element are selected by [4] such that the initial and final velocities of each element can be matched and assumed solution can be evaluated. These trial functions are

$$\phi_1(\sigma_j) = 1 - 3\left(\frac{\sigma_j}{t_j}\right)^2 + 2\left(\frac{\sigma_j}{t_j}\right)^3, \tag{2.18a}$$

$$\phi_2(\sigma_j) = t_j\left[\left(\frac{\sigma_j}{t_j}\right) - 2\left(\frac{\sigma_j}{t_j}\right)^2 + \left(\frac{\sigma_j}{t_j}\right)^3\right], \tag{2.18b}$$

$$\phi_3(\sigma_j) = 3\left(\frac{\sigma_j}{t_j}\right)^2 - 2\left(\frac{\sigma_j}{t_j}\right)^3, \tag{2.18c}$$

$$\phi_4(\sigma_j) = t_j\left[- 2\left(\frac{\sigma_j}{t_j}\right)^2 + \left(\frac{\sigma_j}{t_j}\right)^3\right]. \tag{2.18d}$$

The time in which the cutting-edge is in contact with workpiece, t_c, is divided into E elements such that $t_j = t_c/E$. Time integral is taken for each element. The equation then takes the following form

$$\begin{aligned} \int_0^{t_j} \Bigg[& m\left(\sum_{i=1}^{4} a_{ji}^n \ddot{\phi}_i(\sigma_j)\psi_p(\sigma_j)\right) + c\left(\sum_{i=1}^{4} a_{ji}^n \dot{\phi}_i(\sigma_j)\psi_p(\sigma_j)\right) + \\ & (k - wC_1(\sigma_j))\left(\sum_{i=1}^{4} a_{ji}^n \phi_i(\sigma_j)\psi_p(\sigma_j)\right) + \\ & wC_1(\sigma_j)\left(\sum_{i=1}^{4} a_{ji}^{n-1} \phi_i(\sigma_j)\psi_p(\sigma_j)\right) - wC_2(\sigma_j)\psi_p(\sigma_j)\Bigg] d\sigma_j = 0, \\ & p = 1, 2. \end{aligned} \tag{2.19}$$

where $C_1(t)$ and $C_2(t)$ are replaced by $C_1(\sigma_j)$ and $C_2(\sigma_j)$ to show the dependence on local time.

2.2.2 Free Vibrations

While the cutting edge is not in contact with the workpiece, the system is not forced and experiences free vibration. It can be represented by the equation

$$\ddot{x}(t) + c\dot{x}(t) + kx(t) = 0. \tag{2.20}$$

The solution can be assumed to be

$$x(t) = c_1 e^{\lambda_1 t} + c_2 e^{\lambda_2 t}, \tag{2.21}$$

where

$$\lambda_{1,2} = \frac{-c \pm \sqrt{c^2 - 4mk}}{2m}. \tag{2.22}$$

To represent the change in state when cutting action ends and free vibration begins, the following equation can be used

$$\begin{bmatrix} x(t_c + t_f) \\ \\ \dot{x}(t_c + t_f) \end{bmatrix} = \frac{1}{\lambda_1 - \lambda_2} \begin{pmatrix} \lambda_1 e^{\lambda_2 t_f} - \lambda_2 e^{\lambda_1 t_f} & e^{\lambda_1 t_f} - e^{\lambda_2 t_f} \\ \\ \lambda_1\lambda_2 e^{\lambda_2 t_f} - \lambda_1\lambda_2 e^{\lambda_1 t_f} & \lambda_1 e^{\lambda_1 t_f} - \lambda_2 e^{\lambda_2 t_f} \end{pmatrix} \begin{bmatrix} x(t_c) \\ \\ \dot{x}(t_c) \end{bmatrix}. \tag{2.23}$$

Here, t_f is the time of free vibration and tc is the time when cutting action ends. This equation can be generalized for every period and represented as

$$\begin{bmatrix} x(n\tau) \\ \\ \dot{x}(n\tau) \end{bmatrix} = \mathbf{\Phi} \begin{bmatrix} x((n-1)\tau + t_c) \\ \\ \dot{x}((n-1)\tau + t_c) \end{bmatrix}, \tag{2.24}$$

where $\mathbf{\Phi}$ is the 2x2 matrix from Equation 2.23. Subsequently, the initial and final states of the free vibration can be correlated by

$$\begin{pmatrix} a_{11} \\ \\ a_{12} \end{pmatrix}^n = \mathbf{\Phi} \begin{pmatrix} a_{E3} \\ \\ a_{E_4} \end{pmatrix}^{n-1}, \tag{2.25}$$

where E is the total number of elements in the cut. In order to obtain states for intermediate elements, continuity can be implemented by equating state at the end of one element with that at the beginning of the next element.

2.2.3 Stability Analysis

Stability analysis of the predicted solution can be done by relating the assumed solution to the state of previous tooth passage. This can be done by combining Equations 2.24 and 2.25 to form a global matrix for E=2 [4], given by

$$\begin{bmatrix} 1 & 0 & 0 & 0 & 0 & 0 \\ 0 & 1 & 0 & 0 & 0 & 0 \\ N_{11}^1 & N_{12}^1 & N_{13}^1 & N_{14}^1 & 0 & 0 \\ N_{21}^1 & N_{22}^1 & N_{23}^1 & N_{24}^1 & 0 & 0 \\ 0 & 0 & N_{11}^2 & N_{12}^2 & N_{13}^2 & N_{14}^2 \\ 0 & 0 & N_{21}^2 & N_{22}^2 & N_{23}^2 & N_{24}^2 \end{bmatrix} \begin{bmatrix} a_{11} \\ a_{12} \\ a_{13} \\ a_{14} \\ a_{15} \\ a_{16} \end{bmatrix}^n = \begin{bmatrix} 0 & 0 & 0 & 0 & \Phi_{11} & \Phi_{12} \\ 0 & 0 & 0 & 0 & \Phi_{21} & \Phi_{22} \\ P_{11}^1 & P_{12}^1 & P_{13}^1 & P_{14}^1 & 0 & 0 \\ P_{21}^1 & P_{22}^1 & P_{23}^1 & P_{24}^1 & 0 & 0 \\ 0 & 0 & P_{11}^2 & P_{12}^2 & P_{13}^2 & P_{14}^2 \\ 0 & 0 & P_{21}^2 & P_{22}^2 & P_{23}^2 & P_{24}^2 \end{bmatrix} \begin{bmatrix} a_{11} \\ a_{12} \\ a_{13} \\ a_{14} \\ a_{15} \\ a_{16} \end{bmatrix}^{n-1} + \begin{bmatrix} 0 \\ 0 \\ C_1^1 \\ C_2^1 \\ C_1^2 \\ C_2^2 \end{bmatrix}, \tag{2.26}$$

where Φ_{11}, Φ_{12}, Φ_{21}, Φ_{22} are the elements of $\mathbf{\Phi}$ in Equation 2.26, and

$$N_{pi}^j = \int_0^{t_j} [m\ddot{\phi}_i(\sigma_j) + c\dot{\phi}_i(\sigma_j) + (k - bK_{sx}(\sigma_j))\phi_i(\sigma_j)]\psi_p(\sigma_j)d\sigma_j, \tag{2.27}$$

$$P_{pi}^{j} = \int_{0}^{t_j} -bK_{sx}(\sigma_j)\phi_i(\sigma_j)\psi_p(\sigma_j)d\sigma_j, \tag{2.28}$$

$$C_{p}^{j} = \int_{0}^{t_j} bC_2(\sigma_j)\psi_p(\sigma_j)d\sigma_j. \tag{2.29}$$

The global matrix equation, Equation 2.26 can also be represented in the form

$$\mathbf{A}\,\overrightarrow{a}_n = \mathbf{B}\,\overrightarrow{a}_{n-1} + \overrightarrow{\mathbf{C}}. \tag{2.30}$$

The transition matrix can now be defined as

$$\mathbf{Q} = \mathbf{A}^{-1}\mathbf{B}. \tag{2.31}$$

Eigenvalues of this matrix are also called characteristic multipliers. For a given set of parameters, these eigenvalues should have a magnitude less than unity in order to be asymptotically stable.

2.2.4 Stability Charts' Replication

The stability charts shown in Figures 2.2, 2.3 and 2.4 were produced using a TFEA algorithm. They were produced with same parameters as those by Mann [4] [6] so as to cross-check those with the already validated ones. The general form of autonomous 3^{rd} order DDE used to produce Fig. 2.3 is given by

$$\frac{d^3x}{dt^3} + \alpha\dot{x} + \beta x(t-\tau) = 0. \tag{2.32}$$

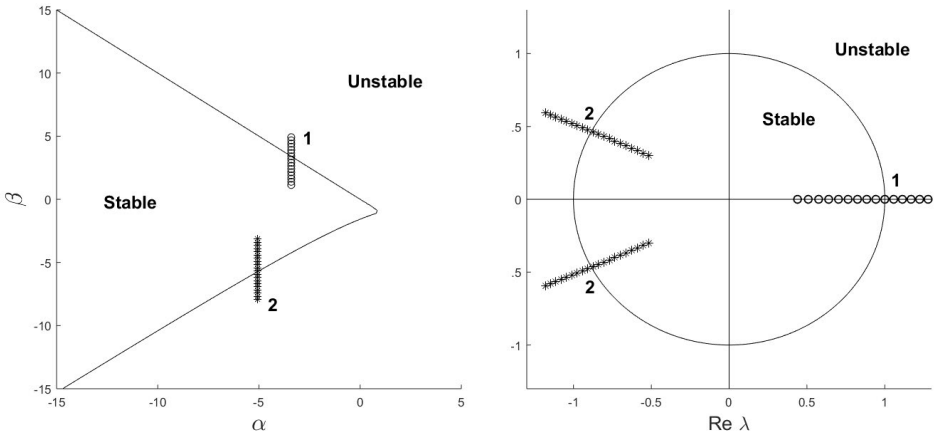

FIGURE 2.2: TFEA applied on scalar autonomous DDE to obtain (a) Converged stability chart using a single temporal element and $\tau = 1$, (b) CM trajectories on complex plane for a range of β with α_1=3.4 and α_2=5.08.

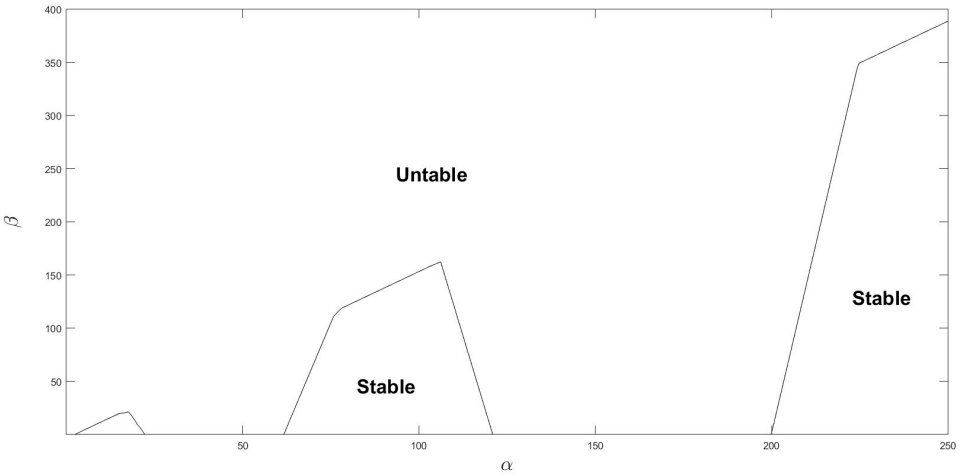

FIGURE 2.3: TFEA applied on autonomous 3^{rd} order DDE for scalar parameters given by Equation 2.32, with $\tau = 1$.

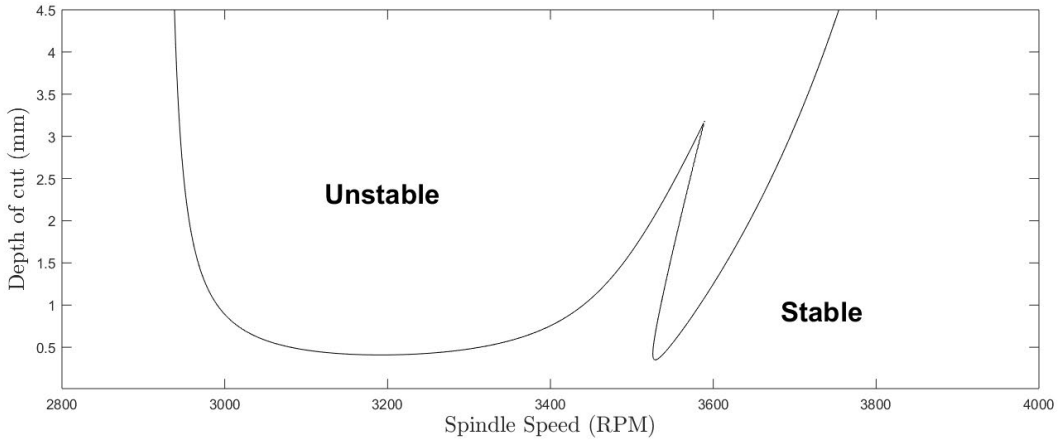

FIGURE 2.4: Stability prediction using TFEA with two elements, for up-milling process with ω_n=920.48 rad/s, K=2.18 x 10^6, ζ=0.0032 and 5% radial immersion. Structured was assumed to be flexible in direction along the feed.

2.3 Spectral Element Analysis

Spectral Element Analysis, or Spectral Element Approach for TFEA, is an extension of TFEA. After describing the global stiffness matrix in TFEA (Eq 2.26), SEA can be implemented. Key aspects of SEA are replacement of integrals by summations and replacement of uniformly distributed nodal points by non-uniform quadrature points. The work is entirely based on the SEA approach developed by Firas et al. [10]. Unlike conventional state-space TFEA, Spectral TFEA developed by him can incorporate hp-convergence and hence have significantly higher convergence rates. This allows analysis of higher order and more complex DDEs by applying numerical quadrature and not analytical integrations. Since this is an approximation technique, equidistance nodes are efficient only for low number of nodes. For higher values, the use of "asymptotically arcsin-distributed" nodes has been suggested [11]. Legendre-Guauss-Lobatto (LGL) points are well-conditioned for this. A major advantage of LGL quadrature is that quadrature values are calculated before obtaining the trial functions. This facilitates faster calculation of intense integrals using the Gauss quadrature. As described in [10], expression for LGL quadrature is given by

$$\int_0^1 f(\eta)d\eta = \sum_{k=1}^{n+1} w_k f(\eta_k) \tag{2.33}$$

where $f(\eta)$ is the integrand from weighted residual method. η_k are the Legendre points transformed to [0, 1] from [-1, 1] using

$$\tilde{u} = \frac{b-a}{2}u + \frac{b+a}{2} \tag{2.34}$$

where $u \in$[-1, 1] and $\tilde{u} \in [a, b]$ Values of $f(\eta)$ at LGL points are denoted by $f(\eta_k)$. w_k are the quadrature weights.

To populate the global matrices, applying LGL quadrature to N_{ij} and P_{ij} terms

from TFEA gives

$$N_{ij}^{p} = \sum_{k=1}^{n+1} \left(\frac{1}{t_j} \mathbf{I} \phi_i'(\eta_k) \psi_p(\eta_k) w_k \right) - \mathbf{A}((\eta_i + j - 1) t_j) \psi_p(\eta_i) w_i \tag{2.35}$$

$$P_{ij}^{p} = \mathbf{B}((\eta_i + j - 1) t_j) \psi_p(\eta_i) w_i \tag{2.36}$$

This enables evaluating the weighted residual integrals without the need to obtain expressions of trial functions. Weights can be obtained by interpolants from within the elements.

Stability Charts Reproduced

The stability charts shown in Figures 2.5 and 3.4 were produced using an SEA algorithm. The algorithm has been prepared using references from the work by Firas et al [10]. The figures are produced with same parameters as those using TFEA for the purpose of comparison. They are found to be identical, hence validating the algorithm.

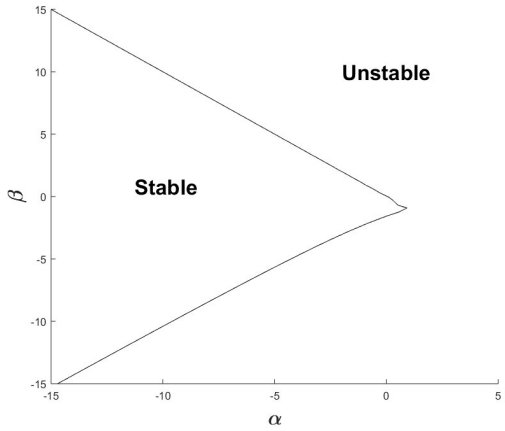

FIGURE 2.5: SEA applied on scalar autonomous DDE to obtain converged stability chart with $\tau = 1$.

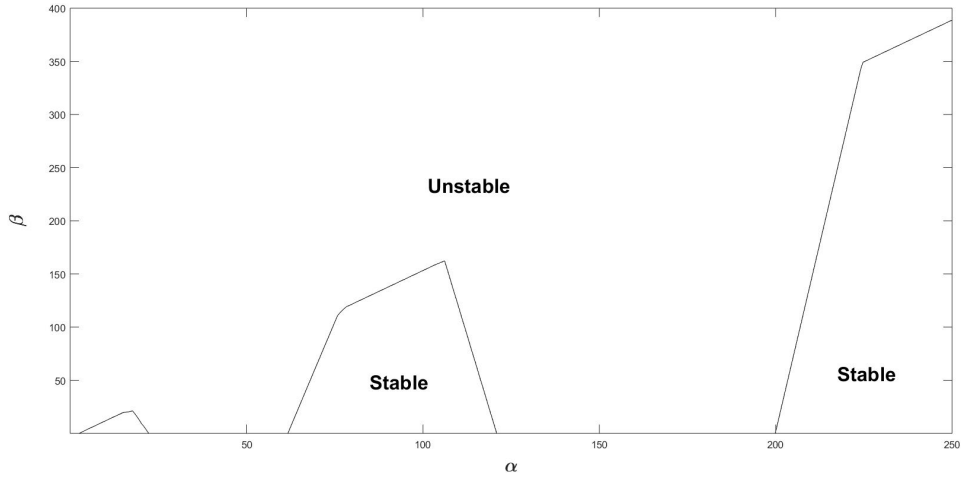

FIGURE 2.6: SEA applied on autonomous 3^{rd} order DDE for scalar parameters given by Equation 2.32, with $\tau = 1$.

3

Experimental Validation of Stability Prediction

3.1 Experiment Setup

Experimental validation of TFEA algorithm and corresponding stability chart is a necessary checkpoint. As shown in Figure 3.1, a setup was designed and manufactured for this purpose. A monolithic unidirectional flexure was used to constrain the motion to just one direction. It was rigid along the planned feed direction, and flexible orthogonal to it. It was designed and manufactured by Mann, B. P. [4]. A dummy semi-machined block was mounted on the flexure as a workpiece to be worked upon, external dimensions being 4.2" x 4" x 1.5". An adapter plate was designed for rigid mounting of the flexure on the CNC machine table. It helped avoid additional vibrations. It also incorporated provisions to allow system modification and to mount the flexure such that flexibility is in direction along the feed. The complete assembly was manufactured out of Aluminum. A Tormach PCNC 440 milling machine was used for all the tests.

There was rigid fastening at workpiece-flexure, flexure-adapter and adapter-CNC table interfaces. Hence, the only significant motion due to vibration was between the

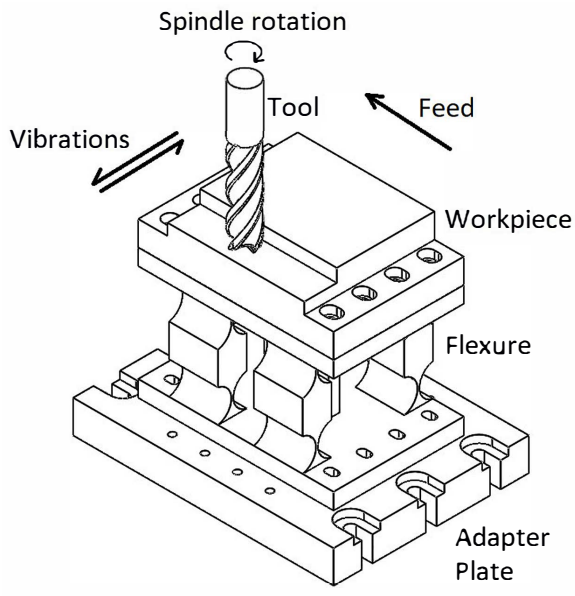

FIGURE 3.1: Schematic diagram of the experimental setup along with feed, vibration and spindle directions.

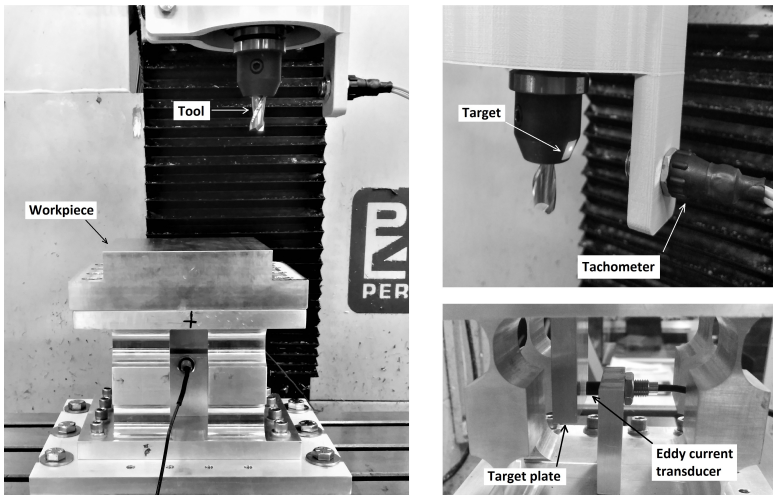

FIGURE 3.2: Clockwise from left: Experimental setup on the CNC bed, Tachometer and mounting arrangement on spindle head, Eddy current transducer arrangement

top and bottom surfaces of the flexure. To get accurate measurements of this relative motion, a non-contact eddy current transducer was used. As shown in Figure 3.2, the transducer was held in a mounting plate which was rigidly attached to the bottom

of the flexure. It measured distance to a target plate which was rigidly attached to the top of the flexure.

During the cutting operation, actual spindle speed is not equal to that set in the CNC G-code. In order to obtain accurate spindle speed during various phases of the cutting operation, a laser tachometer was used. It was mounted on the moving spindle head and targets the tool holder, which is mat-black with one white region. The laser tachometer read this black-white transition to provide a pulse every time it passes through the white region, thus helping estimate the spindle rotational speed. The output of the tachometer and displacement transducer were anti-alias filtered with a sampling rate of 10,000 Hz and read by laptop through a data acquisition unit.

3.2 Modal Parameter Extraction

In order to predict system stability using stability charts, modal parameters of the system are required. They are modal mass, damping ratio, and natural frequency. This was done by performing impact modal tests. An impact modal hammer with nylon tip was used for forcing the system over an infinitesimal time interval, and thus a wide range of frequencies. An accelerometer was used to measure the vibrations. To verify the accelerometer readings, an eddy current transducer was also used. The list of instruments used is as given in Table 3.1, and arrangement was as shown in Figure 3.3

Hammer impact generated vibrations and subsequent relative motion between the top and bottom faces of the flexure. They were measured by the accelerometer and the displacement transducer, respectively. Time domain data from the hammer, accelerometer and eddy current transducer were obtained through a DAQ after signal amplification. Since the acquired time domain data had considerable noise, a Savitzky-Golay filtering technique was used. This digital filter convolutes over

Table 3.1: List of apparatus used in modal tests and cutting trials.

Instrument	Model
Impact Hammer	PCB 086C03
Accelerometer	PCB 352B10
Displacement Transducer	Lion Precision U8B
Tachometer	TTT LT-880
Data Acquisition Unit	NI USB-6251
Signal Amplifier	PCB 482A16

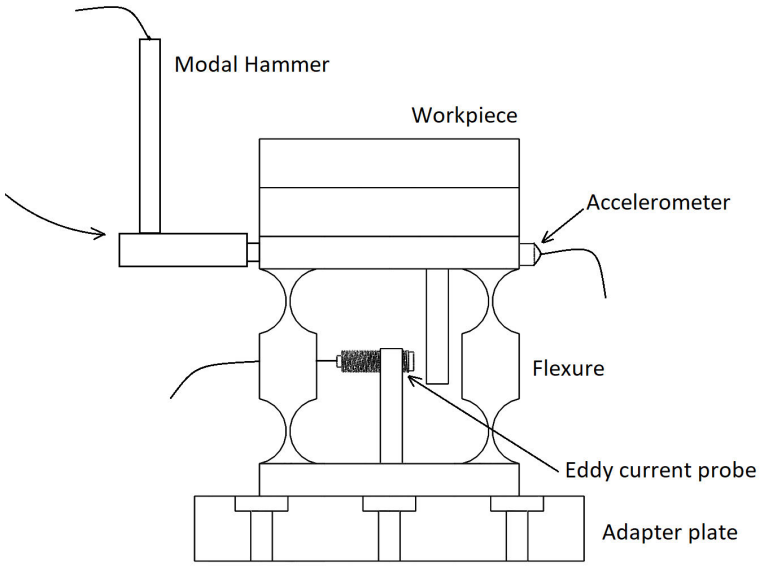

FIGURE 3.3: Schematic diagram of the setup for modal tests.

the data points by fitting moving windows with a low-degree polynomial using the method of linear least squares [12]. Time domain data from one of the modal tests was as shown in Figure 3.4.

From Fourier transform of the time-domain data, as shown in Figure 3.5, damped natural frequency can be obtained. Resolution of the FFT was increased by padding experimental data's time series with zeroes until the change in value was within 0.1%. For estimation of damping ratio, logarithmic decrement method is used with guided windowing technique. Selection of number of periods between two peaks for

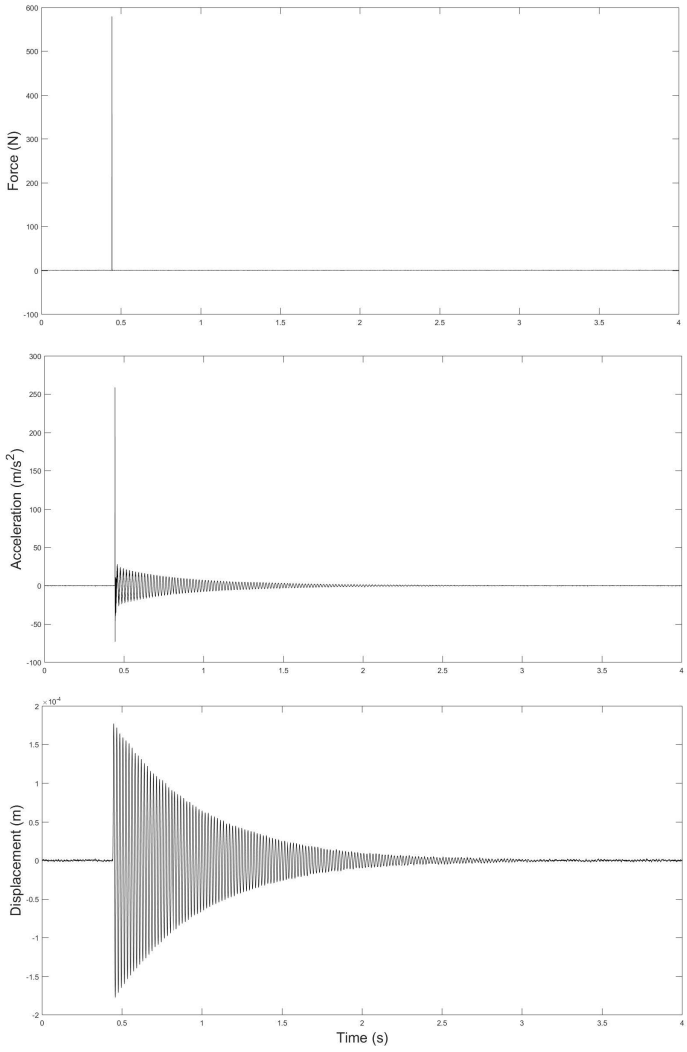

FIGURE 3.4: Time-domain data from modal tests for (a) Impact Hammer, (b) Accelerometer and (c) Eddy current transducer.

logarithmic decrement estimation was driven by the uncertainty propagation method shown in [13]. Then natural frequency can be obtained using

$$\omega_n = \frac{\omega_d}{\sqrt{1-\zeta^2}} \tag{3.1}$$

Furthermore, a Frequency Response Function (FRF), as shown in Figure 3.6, is used for estimation of stiffness. It is obtained by considering output/input ratio in the frequency domain. Analytically, it is known that the transfer function is given

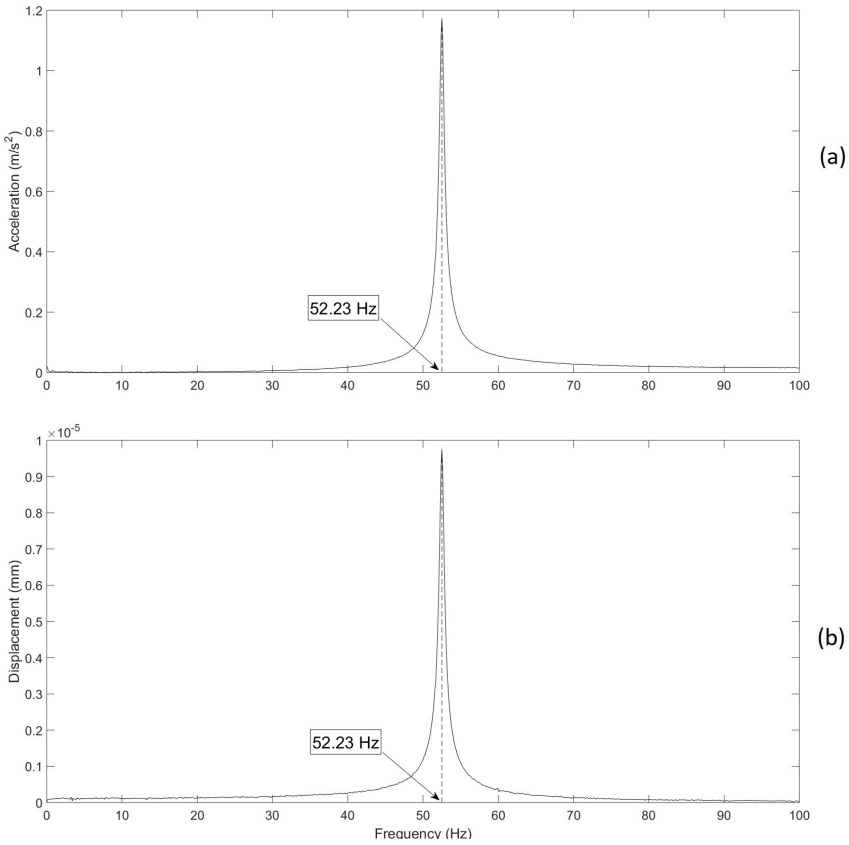

FIGURE 3.5: Frequency-domain data from (a) accelerometer and (b) eddy current probe, showing a peak at the damped natural frequency $\omega_d = 52.23$ Hz.

by Equation 3.2.

$$H(i\omega) = \frac{x}{F} = \frac{1/K}{1 - (\omega/\omega_n)^2 + i2\zeta(\omega/\omega_n)} \tag{3.2}$$

From this, value of k can be estimated for various frequencies, and subsequently the modal mass using

$$m = \frac{k}{\omega_n^2} \tag{3.3}$$

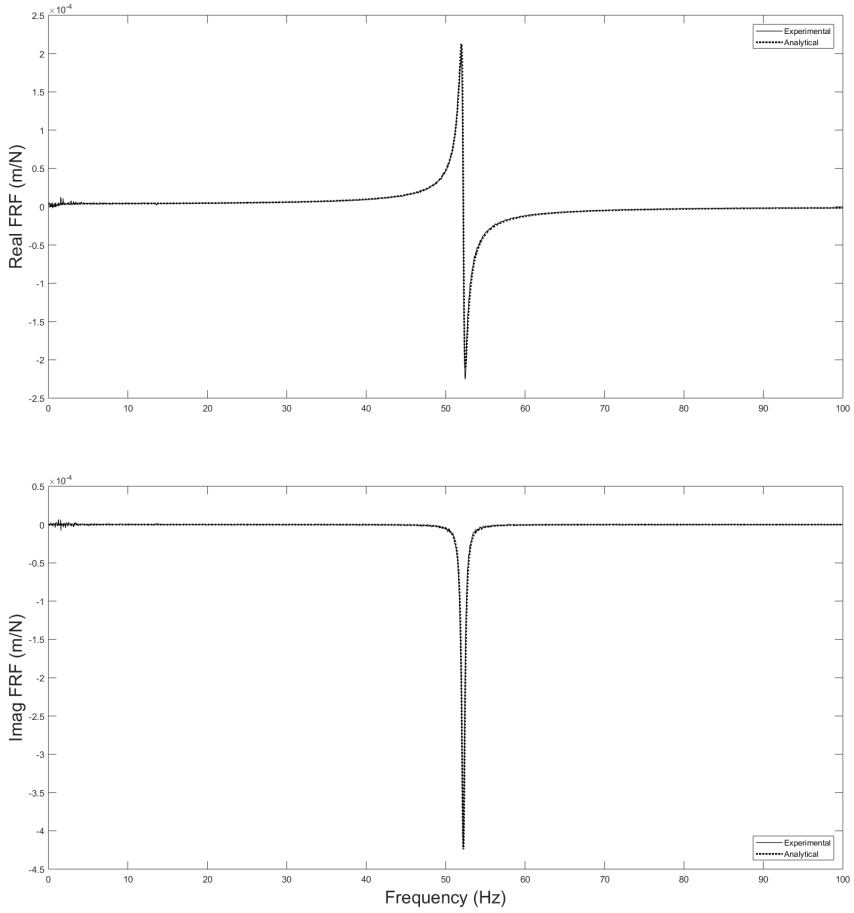

FIGURE 3.6: Comparison of real and imaginary parts of experimental and analytical parts of Frequency Response Functions.

For verification of the damping ratio, $\omega = \omega_n$ was substituted into Eq. 3.2 to obtain

$$\zeta = \frac{1/K}{2Im(H(i\omega)_{\omega=\omega_n})} \tag{3.4}$$

It was observed that the damping ratio from both the methods were in agreement.

The parameters obtained are as listed in the Table 3.2. Values of cutting coefficients in tangential and normal directions were obtained by Mann [4]. They were obtained by analyzing variation in cutting forces with respect to chip loads [14].

The extracted modal parameters were used to produce stability chart for down-milling using a 1/2" single-toothed tool with 30^o helix angle 5% radial immersion.

Table 3.2: Modal parameters extracted from impact hammer modal test results.

Parameter	Value
Natural frequency (ω_n)	328.17 rad/sec
Damping Ratio (ζ)	0.0047
Damping coefficient (c)	7.18 N sec/m
Stiffness (k)	250748 N/m
Modal mass (m)	2.33 Kg
Tangential cutting coefficient (K_t)	5.36 x 10^8 N/m^2
Normal cutting coefficient (K_n)	1.87 x 10^8 N/m^2

It considered a feed rate of 5/1000 inches/tooth passage. Figure 3.10 shows the stability chart for given system, based on extracted parameters.

To analyze the criticality of extracted parameters in predicting the stability, comparisons were made for errors in prediction of ω_n, ζ, K_n and K_t values. It can be seen in Figure 3.7 that an error of $\pm 1.5\%$ in determining ω_n considerably changes the predicted stability. And an error of $\pm 10\%$ in obtaining cutting constants can drastically modify the high speed stability patterns. However, even an error of $\pm 15\%$ in determining ζ does not have a significant deviation in the prediction.

To verify if the modal parameters depend on the position of CNC bed, multiple tests were done at various bed locations. However, the parameters were in agreement with each other with negligible variation of less than 0.1%.

3.3 Cutting Tests

Modal parameters extracted from the impact hammer tests were used to prepare stability charts and predict stability for a range of combinations of spindle speeds and depths of cut. For down-milling with 5% radial immersion using a 1/2" single flute end-mill with 30° helix angle, the stability chart is as shown in Figure 3.10.

Based on the stability chart predictions, single-pass cutting tests were performed for various parameter combinations. It was observed that actual spindle speed was

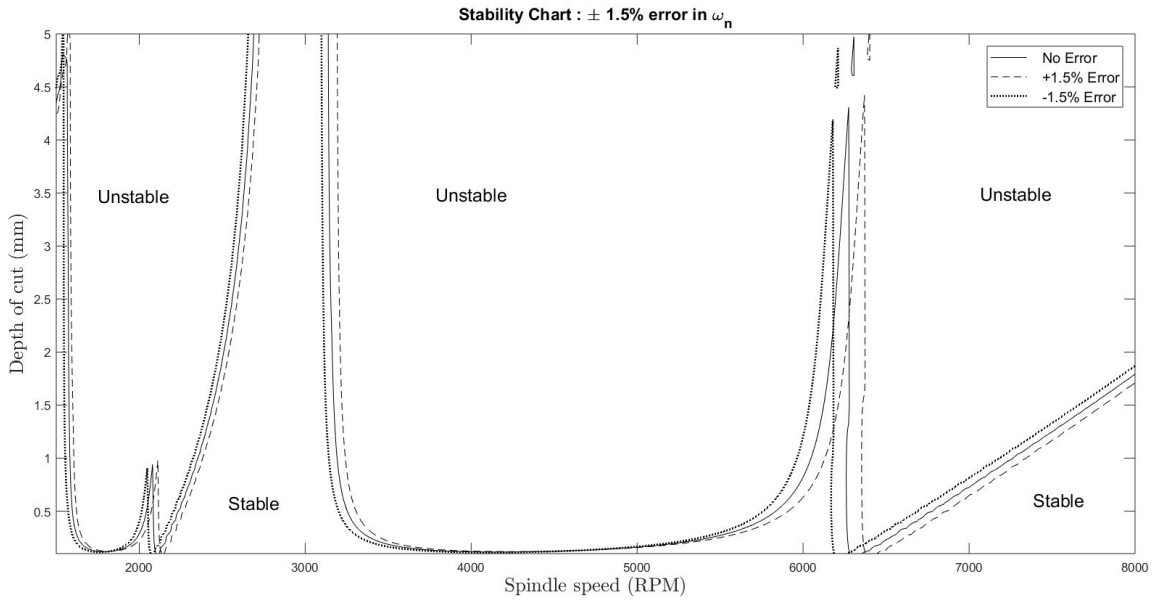

FIGURE 3.7: Shift in stability boundaries with an error of $\pm 1.5\%$ in ω_n estimation. A significant deviation of the boundaries can be seen over the complete range of parameters.

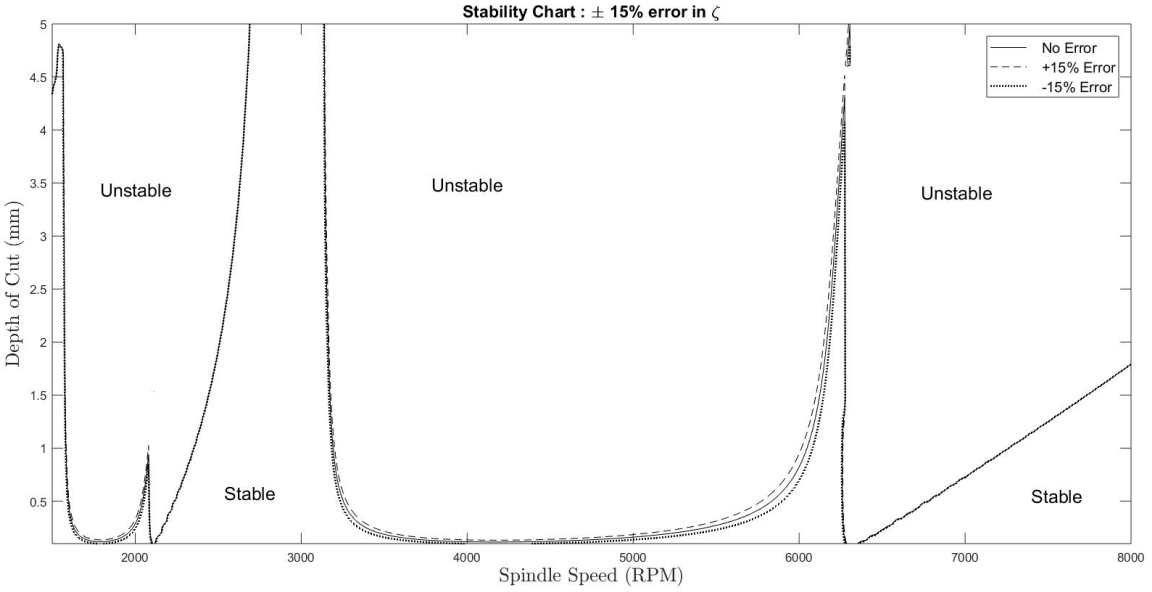

FIGURE 3.8: Shift in stability boundaries with an error of $\pm 15\%$ in ζ estimation. Deviation of the boundaries is not significant and can be considered negligible.

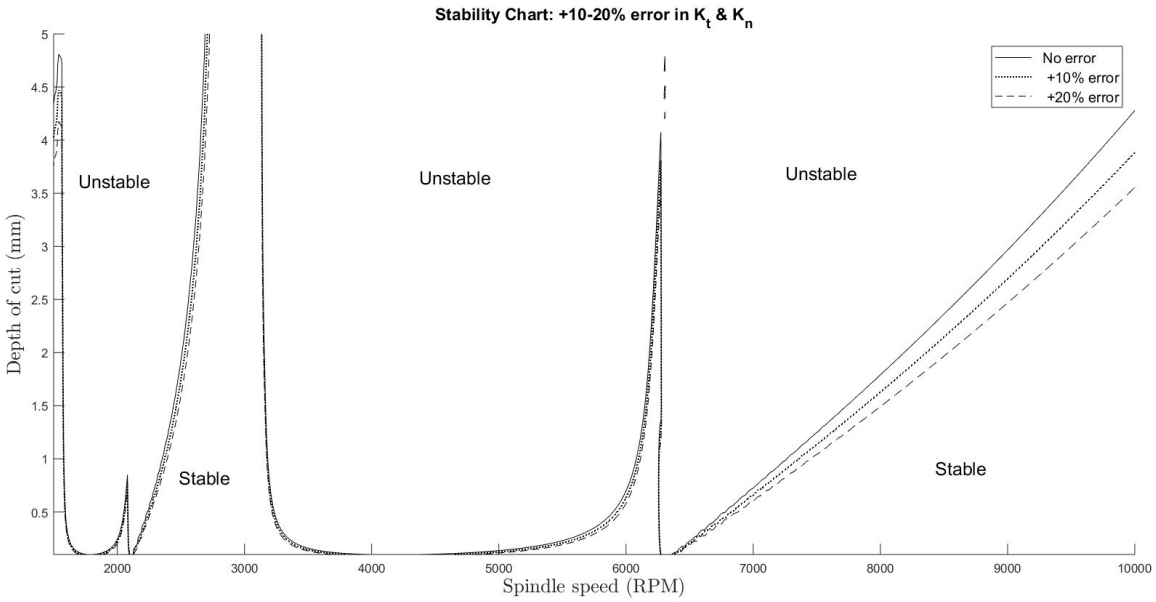

FIGURE 3.9: Shift in stability boundaries with an error of 10-20% in K_t & K_n estimation. Deviation in boundaries is negligible at low spindle speeds, but significantly larger at high speeds.

considerably more than the speed set in CNC controller. Hence, using a tachometer was important. Real-time spindle speed and flexure displacement data were obtained through tachometer and eddy current transducer, respectively. It is known that for stable vibrations, displacement due to cutting vibration remains constant for each tooth passage [4]. Stroboscopic samples (1/rev displacement points) were obtained from the time-domain data to observe the displacement at a particular tool angle during each rotation. Also, Poincare sections were prepared which show the displacement during n^{th} tooth passage with respect to that during $(n-1)^{th}$ tooth passage. Stable cuts had stroboscopic points along a steady constant line and Poincare section with points highly concentrated at the origin. Whereas unstable cuts had stroboscopic points not in synchronization with tooth passage and Poincare section with points arranged in a circular manner. Moreover, certain data sets belonged to neither of the two categories and need significantly intense investigation and analysis. For

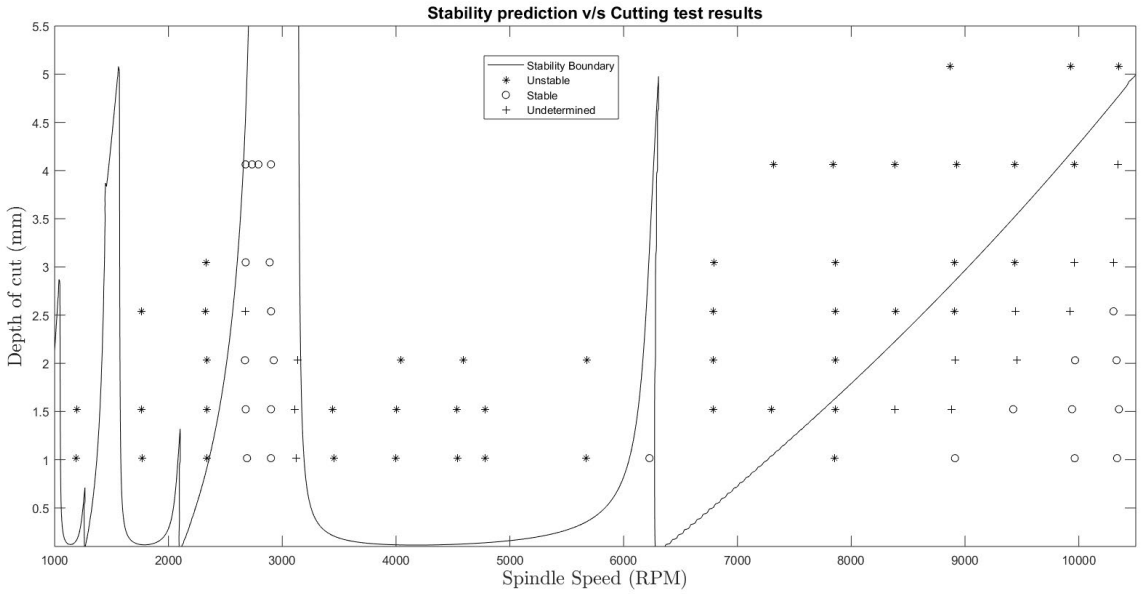

FIGURE 3.10: Stability prediction for the experimental setup from extracted modal parameters v/s stability data obtained from experimental cutting data. Stability charts corresponds to down-milling with 5% radial immersion using a 1/2" single flute end-mill with 30◦ helix angle, with modal parameters from Table 3.2. The asterisks represent unstable cuts, circles represent stable cuts and plus signs represent cuts that were not determined to be either of the two.

this thesis, they have been labelled as undetermined.

Figures 3.11, 3.12 and 3.13 show continuous sampled data, stroboscopic data and Poincare sections for stable, unstable and indeterminate cutting test data. Figure 3.14 shows milled cuts for a highly unstable and a stable cut. In case of highly unstable cut, the waviness is evident and can be visually identified. However, the majority of the other types of cuts cannot be identified by visual inspection. Fig. 3.13 shows some cuts which cannot be classified into either of the two categories. Fig. 3.13 (a) suggests period doubling at steady state where TFEA model has negative CM with magnitude greater than unity. In this case, the displacement is constant for every alternate tooth passage. Whereas Fig. 3.13 (c) shows a stable state being achieved towards the end of the cut. Further detailed analysis of the indeterminate data is required.

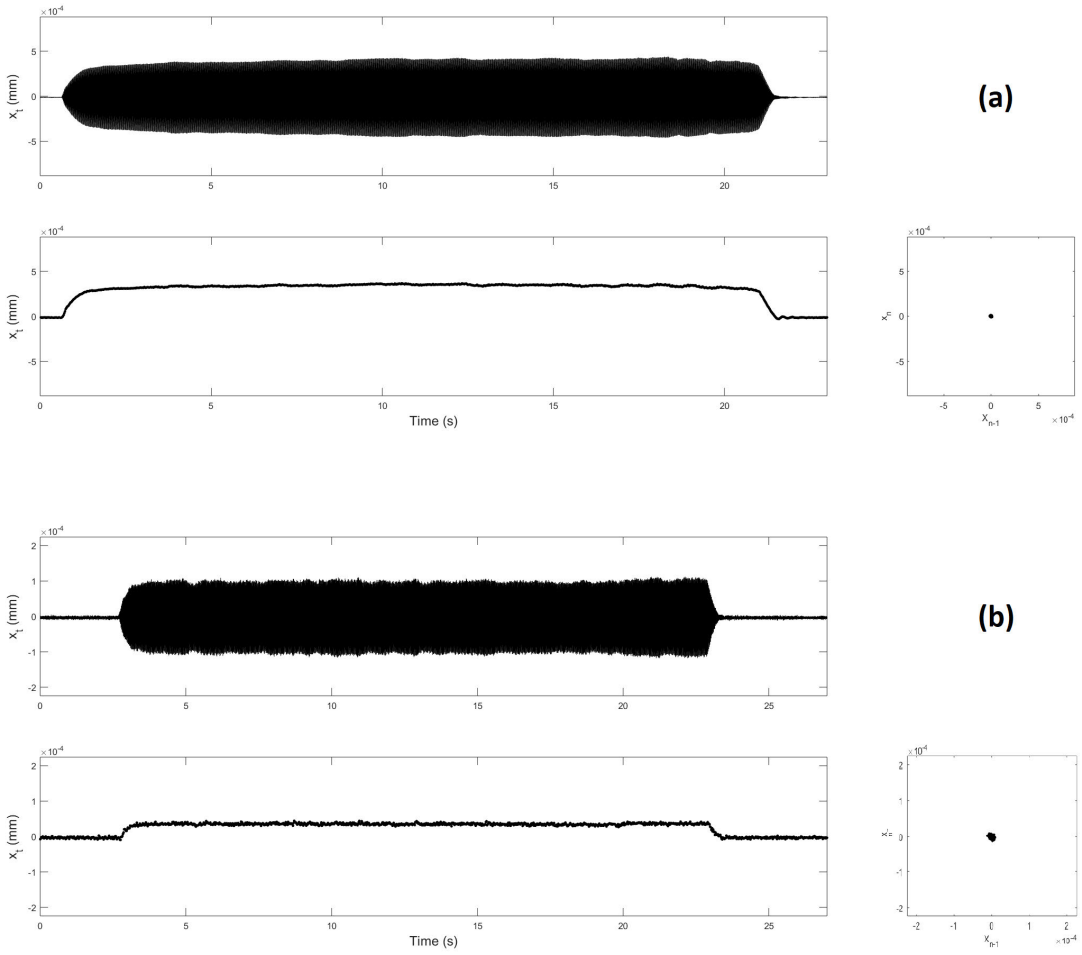

FIGURE 3.11: Continuous, Stroboscopic and Poincare plots of the stable cuts for experimental data corresponding to (a) Ω=2900 rpm, w=0.04 in (b) Ω=2900 rpm, w=0.16 in.

Based on this analysis, the data points were plotted over stability prediction and compared. As it can be seen in Fig. 3.10, the majority of low spindle speed data points are in agreement with the predictions. However, high speed data points differ at certain locations near the stability boundary. Possible reasons for this disagreement are discussed in following sections.

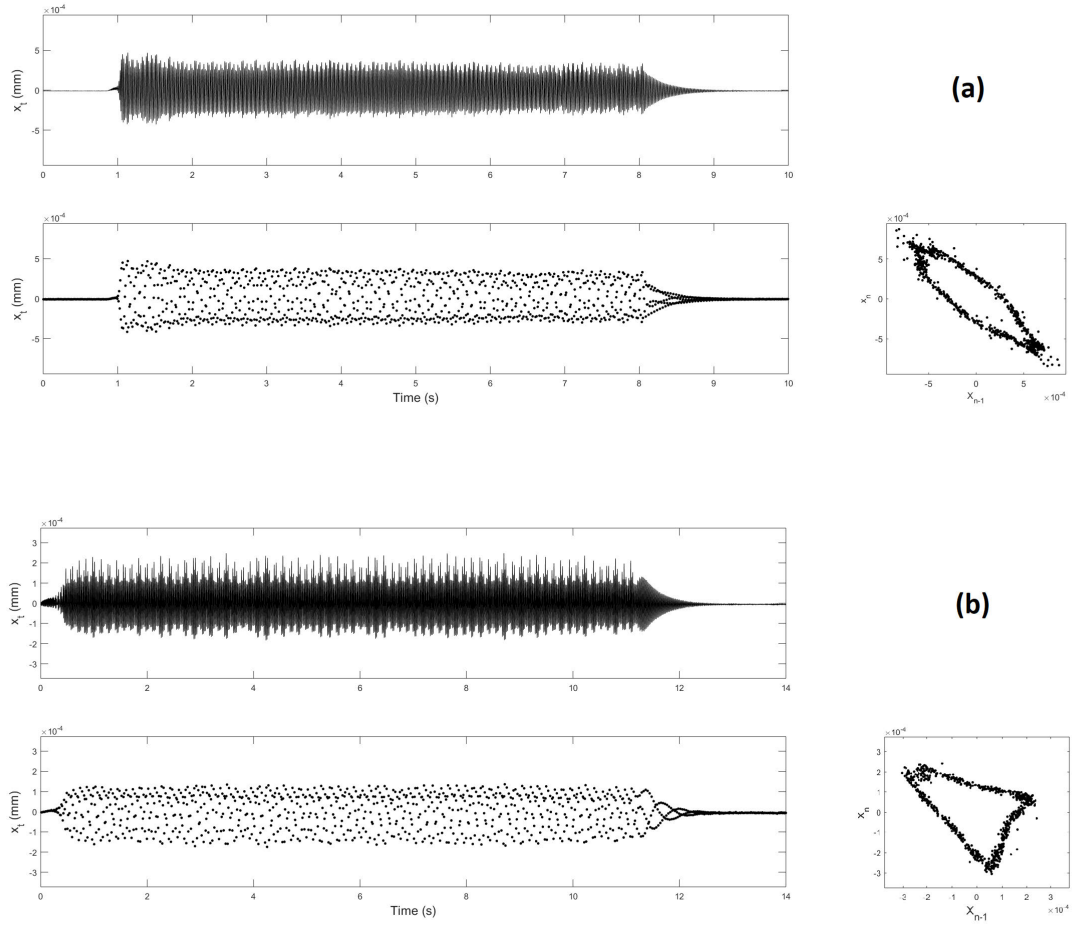

FIGURE 3.12: Continuous, Stroboscopic and Poincare plots of the unstable cuts for experimental data corresponding to (a) Ω=4783 rpm, w=0.06 in (b) Ω=7842 rpm, w=0.16 in.

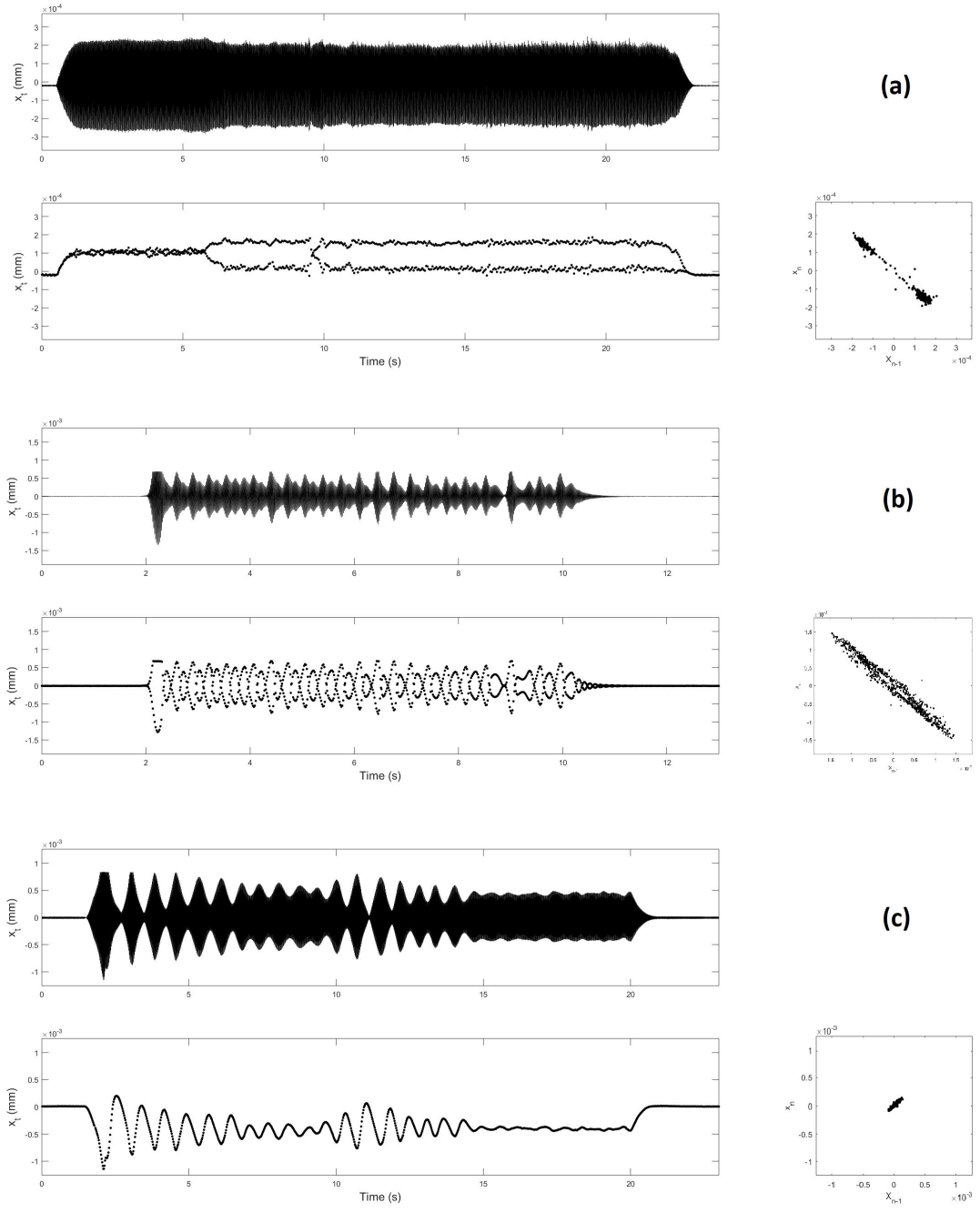

FIGURE 3.13: Continuous, Stroboscopic and Poincare plots of the indeterminate cuts for experimental data corresponding to (a) Ω=6792 rpm, w=0.12 in (b) Ω=2678 rpm, w=0.10 in (c) Ω=3124 rpm, w=0.04 in.

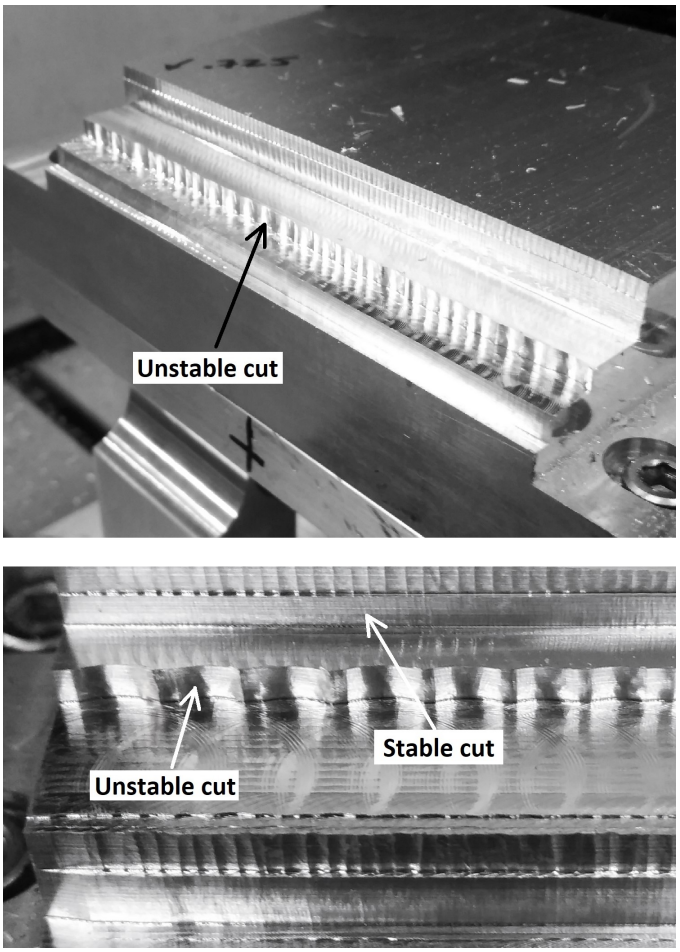

FIGURE 3.14: Comparison of mill pass quality for unstable and stable cuts.

3.4 Sources of Error

Results obtained from the cutting tests are not in accordance with the predictions. This can be attributed to one of the factors discussed in this section.

3.4.1 Tool Dynamics

For the purpose of modelling the system and experimental analysis, it has been assumed that the system has 1 DOF and dynamics of only the workpiece is significant. Tool is assumed to be significantly stiffer and hence its dynamics have been ignored. To verify this assumption, modal tests were carried out on the tool with an intention of estimating stiffness from the FRFs. Figure 3.15 and 3.16 show the time-domain and frequency-domain data of the accelerometer output. It can be seen that the system frequency for tool is considerably higher than those of workpiece. However, natural frequency could not be determined using the data obtain from modal tests.

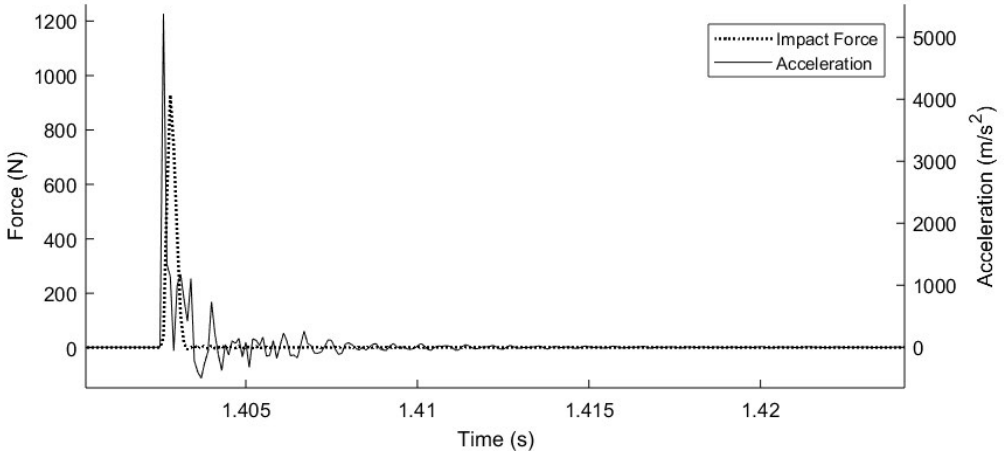

FIGURE 3.15: Tool modal test

It can be seen that the system frequency for tool is considerably higher than that of the workpiece. However, natural frequency could not be determined using the data obtain from modal tests. This can be attributed to various probable factors. First,

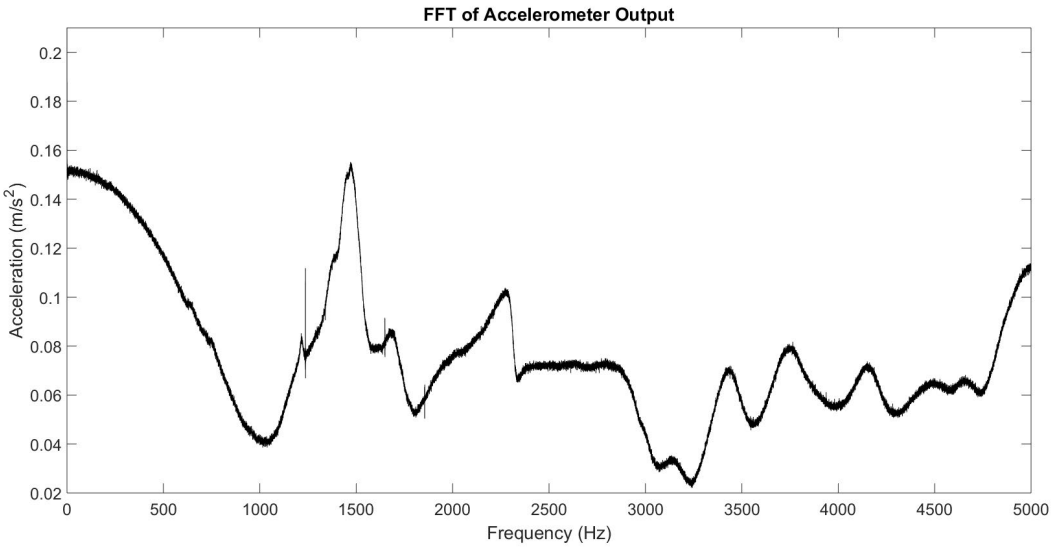

FIGURE 3.16: Frequency domain data from accelerometer.

the tool had a slenderness ratio not low enough to hold the high stiffness assumption. Second, the tool was screwed in the holder and not using a spring collet. It can cause unwarranted motion and an added degree of freedom. Moreover, holding the tool with a grub screw can lead to eccentricity with respect to the CNC spindle center and alter the dynamic forces on the chip. Third, the data acquisition frequency might not have been enough for the given system which operates at a comparable frequency.

3.4.2 Modal Parameters

As described in the previous chapter, an error of even 1.5% in determining the natural frequency of the system can lead to a significant change in the stability chart. Natural frequency was determined using the data from an eddy current displacement transducer. Calibration errors, signal noise and absence of a shield on the transducer probe are some of the factors that could alter the response of modal tests. Also, it was observed that the movement of CNC machine bed caused a small change in damped natural frequency. This change was neglected in stability prediction.

Another source of error can be the cutting coefficients. For this thesis project, they were not obtained practically but used from past research. Even a small deviation in material grade or internal grain structure can alter the stiffness coefficients. This is dominant particularly at high speeds, particularly near the region where experimental data points did not agree with the predictions.

3.4.3 Chip Dynamics

For this study, chip dynamics have not been considered. Kim et al. [15] showed that in this process, chip generation and removal are intermittent. And an interference between the forced vibrations and chatter can cause variation in chip thickness and dynamic forces at the tool-workpiece interface. This can lead to added vibrations in a direction along the feed, which was not modelled for this system. Also, the material was assumed to be homogenous and isotropic. A violation of this assumption can also alter stability predictions.

3.4.4 Varying Feed Rate

Stability prediction assumed a constant feed rate of 5x10^{-3} inches/tooth passage. Feed rate of trial cut was set using the relation:

$$Feed(in/min) = Feed(in/tooth) * SpindleRPM(rev/min) * N(teeth/rev) \quad (3.5)$$

It was observed that actual spindle RPM was drastically different from the set RPM, with difference ranging from 20% to 30%. Whereas the feed rate was set in accordance with the set RPM. This led to a deviation in feed rate with respect to the ideal assumed value and can be a potential cause for disagreement in experimental v/s predicted data for cases near the stable-unstable border.

4

Conclusions

This Master's Thesis project was focused on preparing a Temporal FEA algorithm to predict stability of milling operations, and developing an experimental setup to validate the same. The setup was successfully designed, manufactured and tested on a CNC mill. Also, the TFEA algorithm was developed and tested to predict stability. It can be said that the algorithm was considerably accurate, with scope for improvement. Its results were tested against experimental data sets. For low speeds, the mill cut data was in complete agreement with predicted stability. However, certain data sets at high speeds were in disagreement.

This research suggested that having a 1-DOF assumption was not sufficient and there is a need to model a second DOF. Moreover, a complete math model also needs to incorporate chip dynamics for precise stability predictions at high speeds. Similarly for the case of stability prediction for DDEs, it was observed that Spectral Element Analysis is faster and less computationally intensive because of its ability to incorporate hp-convergence. Modelling SEA for milling operation including tool and chip dynamics can result in faster convergence with robust stability prediction algorithm and significantly reduced deviation from experimental results.

Future research on this problem statement can start with modelling for tool dynamics and developing a Spectral EA code to predict milling stability, with tool-helix considerations. Further, modal parameter extraction procedure can be optimized by use of vibration data from single-pass mill cuts and not modal tests. Long-term goal of this research can be to develop a standard accurate process and algorithm for parameter optimization of milling for any given tool-workpiece combination. Future experimental work can be built upon this research and continue work on the problem statement, at Duke University

Bibliography

[1] Altintas Y (2012) Manufacturing automation: metal cutting mechanics, machine tool vibrations, and CNC design. Cambridge university press

[2] Tlusty J (2000) Manufacturing processes and equipment

[3] Stépán G (1989) Retarded dynamical systems: stability and characteristic functions. Longman Scientific & Technical

[4] Mann BP (2003) Dynamic models of milling and broaching. PhD thesis, Washington University

[5] Martellotti M (1941) An analysis of the milling process. Trans ASME 63:677

[6] Patel B, Mann B, Young K (2008) Uncharted islands of chatter instability in milling. International Journal of Machine Tools and Manufacture 48(1):124–134

[7] Mann B, Patel B (2010) Stability of delay equations written as state space models. Journal of vibration and control 16(7):1067

[8] Virgin LN (2000) Introduction to experimental nonlinear dynamics: a case study in mechanical vibration. Cambridge University Press

[9] Bayly PV, Halley JE, Davies MA, Pratt JR (2001) Stability analysis of interrupted cutting with finite time in the cut. In: ASME International Mechanical Engineering Congress & Exposition, vol 11

[10] Khasawneh FA, Mann BP (2011) A spectral element approach for the stability of delay systems. International Journal for Numerical Methods in Engineering 87(6):566–592

[11] Bloom T, Lubinsky DS, Stahl H (1992) Interpolatory integration rules and orthogonal polynomials with varying weights. Numerical Algorithms 3(1):55–65

[12] Schafer RW (2011) What is a savitzky-golay filter?[lecture notes]. IEEE Signal processing magazine 28(4):111–117

[13] Tweten DJ, Ballard Z, Mann BP (2014) Minimizing error in the logarithmic decrement method through uncertainty propagation. Journal of Sound and Vibration 333(13):2804–2811

[14] Halley JE (2000) Stability of low radial immersion milling. PhD thesis, Washington University

[15] Kim CJ, Mayor JR, Ni J (2004) A static model of chip formation in microscale milling. Journal of manufacturing science and engineering 126(4):710–718